Solid State Ionics 398 (2023) 116269

Contents lists available at ScienceDirect

Solid State Ionics

journal homepage: www.elsevier.com/locate/ssi

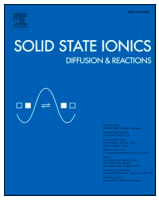

A brick layer model for surface conduction in porous ceramics

Truls Norby [a,*], Xinwei Sun [a], Einar Vøllestad [b]

[a] Department of Chemistry, University of Oslo, Centre for Materials Science and Nanotechnology (SMN), Gaustadalléen 21, NO-0349 Oslo, Norway
[b] Sustainable Energy Technology, SINTEF Industry, Forskningsveien 1, NO-0373 Oslo, Norway

ARTICLE INFO

Keywords:
Oxides
Porous
Surface conductance
Surface protonic conduction
Specific surface area
Brick layer model
ZrO_2
CeO_2

ABSTRACT

We provide herein a review and in-depth derivation and discussion of a surface brick layer model (SBLM) that scales the conductance of a surface layer – such as protonic conductance in adsorbed water – and the macroscopic conductivity for the porous material. The model is derived on basis of grains and pores of similar sizes and will be most realistic for porous compacts or loosely sintered ceramics of isotropic grains, although it still provides order-of-magnitude guidance also for textured or less porous materials. Brief comparison is made with other relevant models and literature. The model is illustrated and evaluated with data primarily from measurements of surface protonic conduction in porous nanoscopic ceramic oxides.

1. Introduction

The surfaces of solids tend to exhibit enhanced transport due to weaker and fewer bonds, more defects, segregation of impurities and dopants, and adsorption and dissociation of gases. Adsorption of water is particularly important as it gives rise to surface protonic conduction that limits the resistance of ceramic insulators. Recently, there is interest in the diffusion and migration of protons in chemisorbed and physisorbed water layers because of implications for heterogeneous catalysis [1–3] and role in mass transport on electrodes for solid-state photoelectrochemical applications [4,5] and proton ceramic fuel cells and electrolysers. [6,7] Based on their surface protonic conductivity, porous ceramics may also be considered as electrolytes in low-drain single chamber or implantable fuel cells, [8–11] electrochemical pumps, humidity sensors, [12,13] and memristive switching. [14]

For many types of surface conduction, such as protonic conduction in chemisorbed or physisorbed water, and for conduction in surface or subsurface layers of the solid, we may theoretically assess concentrations and charge mobilities of charge carriers and hence calculate the conductivity in the layer, or via its effective thickness calculate the in-plane conductance of the layer. This surface conductance can in principle be measured in model systems with well-defined geometries, such as interdigitated electrode arrays on single crystal or ceramic substrates. Our interest now is however to use such theoretical predictions or model measurements of surface conductance to predict the conductivity of a porous material where the geometries are less well-defined or even ill-defined like in a porous sintered ceramic. And, vice versa, from measurement of the conductivity of a porous material with predominant surface conduction to assess the in-plane surface conductance.

Stub *et al.* [15,16] treated surface protonic conduction based on own measurements and standard models for adsorption and transport terms for Y_2O_3-doped ZrO_2 developed by Raz *et al.* [17] but did not attempt to couple it quantitatively to the conductivity of porous samples via the microstructure. Gregori *et al.* [18] introduced a simple model to evaluate surface protonic conduction in ceramics with small amounts of open porosity, and to our knowledge that is the work with the closest relevance to our recent models that we review here, and we shall return to it later.

We here present a surface brick layer model (SBLM) to deduct geometric and mathematical relations that may be used for order-of-magnitude conversions between surface conductance and the measured macroscopic sample conductivity of a porous material. They first appeared in our publication on surface protonic conduction in porous ZrO_2 [19] (see especially its Supplementary Information, SI) and was subsequently expanded and used for interpretation of surface protonics in porous CeO_2. [20] In our present review, the models are derived and discussed in more depth.

There is earlier literature with treatises of conducting interfaces between grains, [21,22] as well as grains covered with a second phase that offers parallel admittance and series impedance [23], both with some geometrical relevance to our present models. However, our approach bears more resemblance to and is inspired by, but still distinct

* Corresponding author.
E-mail address: truls.norby@kjemi.uio.no (T. Norby).

https://doi.org/10.1016/j.ssi.2023.116269
Received 30 March 2023; Received in revised form 12 May 2023; Accepted 23 May 2023
Available online 2 June 2023

from a brick layer model (BLM) for analysis of grain boundary impedance in ceramics. [24] We therefore named it as such originally in the works on ZrO_2 [19] and CeO_2 [20], but are coming to the conclusion that the derivation, results, and uses are sufficiently different that it is better to take a distinctive term (SBLM) into use.

2. Surface conduction and other contributions

The purpose of this paper is not a full treatment of all conductivities and impedances that may contribute in addition to surface conduction, but we provide next a brief consideration of some of them and how they are different and may be separated from the surface conduction we focus on here.

The conduction over the outer surface of a dense or porous material and the conduction on internal surfaces of a porous material is for our purpose the same thing. Surface conduction along closed porosity may contribute to measured conduction by partially short-circuiting the material's bulk conductivity. Here we choose to neglect this, making our treatment most relevant for openly porous materials.

The surface conduction comes in parallel with bulk conduction and parallel grain boundary conduction. Traditionally, they cannot be delineated by impedance spectroscopy, but through variations in microstructure (grain size and porosity) and distinct dependencies on temperature and atmosphere (e.g., wet vs dry when it comes to conduction in adsorbed water).

It has recently been realized that surface conduction in porous ceramics often exhibits two time constants in the regime of geometric capacitances, and this has been assigned to conduction over the convex belly of grains (with higher parallel capacitance from the dielectric material) in series with conduction over the concave neck (with lower parallel capacitance from the gas phase). [19] This is suggested to be a fingerprint of surface conduction, which may have contributions from protonic or other ionic as well as electronic charge carriers. [19,20] In our context here, the surface conduction is obtained from the sum of the resistances of the transport over the lower-frequency convex grain belly part and the higher-frequency concave grain neck part. For the SBLM we are about to derive here, it has no immediate further consequence.

Bulk conduction in the grain interior of a polycrystalline material can have a series resistance from grain boundaries, separable by impedance spectroscopy. It has been discovered that also surface conduction in some materials exhibits a response with capacitances and time constants typical of grain boundary resistance, and Stub *et al.* [15,16] assigned this to what they termed *inter*-grain surface conductance over the grain boundary, in series with the *intra*-grain conductance over the surface of the grain itself. They attributed the inter-grain resistance in the surface conduction to the depletion of protonic charge carriers in the adsorbed water layer at the intersection of the positive space charge of the grain boundary with the negative space charge of surface. [16]

Measurements of surface conductance – like any other conductance – may involve impedances from electrodes. They can be delineated by impedance spectroscopy on two-electrode samples, or they can be eliminated by 4-electrode measurements, given certain requirements that we will not detail here.

3. Simple geometrical aspects of surface conductance

3.1. Surface layer: charge mobility, concentration, conduction

The surface layer with the enhanced conduction can be a subsurface layer, the very solid-gas interface itself, or one or more layers of adsorbed species. In reality, it will often be a combination. In our treatment, we need not differentiate between these cases. The surfaces that contribute to the measured conductivity may be considered to have effectively one surface layer with one in-plane conductance.

The in-plane conductance of the surface layers may be related to their volume conductivity. However, we normally don't know the volume concentration of charge carriers in the layer, and we will not need the volume conductivity *per se*. We will, on the other hand, come to know the surface concentration (e.g., in terms of coverage or number per unit area) and that is eventually what we need to know in order to obtain the in-plane conductance of the surface layer. Now, we still start off with the volume conductivity of the layer in order to stay with familiar terms. The conductivity for a charge carrier i in the volume of a surface layer follows the general expression

$$\sigma_i = z_i F u_i c_i \tag{1}$$

where σ_i is the conductivity with SI units S/m, z_i is the number of charges, u_i is the charge mobility with units of m^2/Vs, and the volume concentration c_i has units of mol/m^3. The in-plane conductance in S of a square sheet of a surface of thickness t_s in m, and width = length = w is

$$G_{s,i} = \sigma_i \frac{w}{w} t_s = \sigma_i t_s = z_i F u_i c_i t_s = z_i F u_i \gamma_i \tag{2}$$

where we in the rightmost expression have replaced the volume concentration c_i with surface concentration γ_i (in mol/m^2) and layer thickness t_s in $c_i = \gamma_i/t_s$. For protons, as an example, the surface protonic conductance of a layer becomes

$$G_{s,H^+} = F u_{H^+} \gamma_{H^+} \tag{3}$$

3.2. Conductivity of porous materials

The surface conductance G_s can be connected to the macroscopic conductivity σ_M for the porous material via a geometry factor that we shall denote ψ (psi) and which has units of 1/m:

$$\sigma_M = \psi G_s \tag{4}$$

ψ will depend on the geometry and percolation of surface pathways, related to the density, grain and pore sizes, and texture.

3.2.1. Materials with columnar or structural pores

Before we dive into porous ceramic materials with randomly organised grains and pores as in compacts and sinters, let us first consider ideally columnar ("c") materials, in which pores are parallel and infinitely open. These may then be one-dimensional (1D) like in anodically grown nano-tubular TiO_2 or in porous layers grown columnarly in pulsed laser deposition (PLD) or in membranes with unidirectional pores, or they may be three-dimensional (3D) possibly including so-called microporous materials with structural porosity, notably zeolites and metal-organic frameworks (MOFs), if a surface conductance can be defined in those structural pores.

3.2.1.1. 1D columnar porosity. For conduction on surfaces in the direction of the columnar pores, simple geometric considerations regardless of the cross-sectional shape of the pore shows that the macroscopic surface conductivity σ_M of the porous material is directly proportional to the volume-specific surface area A_v of the columnar pores, with units of, e.g., m^2/m^3:

$$\sigma_{M,c} = \psi_c G_s = A_v G_s \tag{5}$$

As an example, consider a cubic sample of unit dimensions, divided into $(1/d_g)^3$ cubic grains with grain size d_g (Fig. 1). In the direction of measuring the conductivity, each grain corner is penetrated by square or circular pore columns of width or diameter w_c (Fig. 1).

For square pore columns, each has a circumference of $4w_c$ and depth d_g through the layer and hence conductance $4w_c G_s/d_g$. Each grain contributes one such corner column and the total conductance through an entire layer is proportional to the number of grains $(1/d_g)^2$ and hence $(4w_c G_s/d_g)(1/d_g)^2 = 4w_c G_s/d_g^3$. The conductivity through the unit cube and hence macroscopic conductivity is then $\sigma_{M,c} = (4w_c G_s/d_g^3)/(1/d_g) = 4w_c G_s/d_g^2 = \psi_c G_s$. The volume specific surface area (of the cube) is $A_v =$

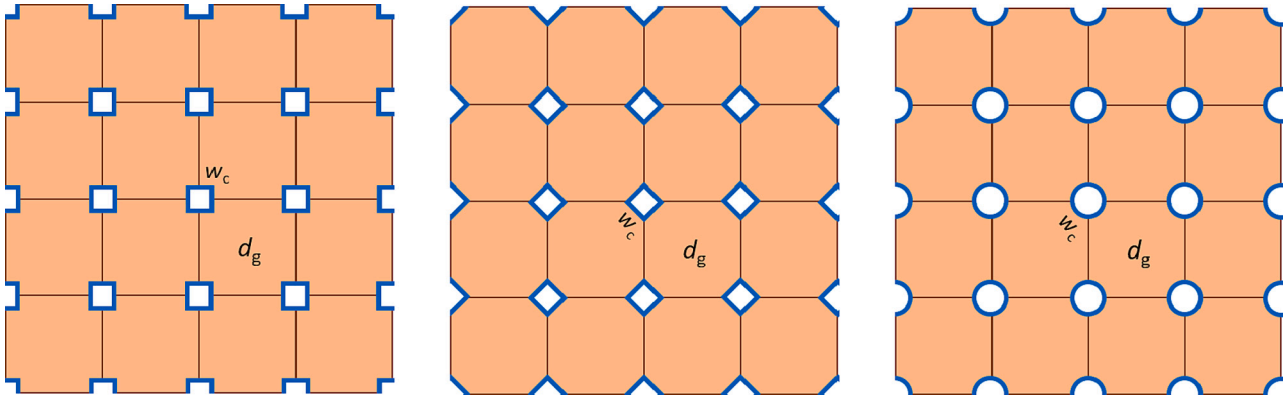

Fig. 1. Schematic representations of 1D columnar porosity in the plane perpendicular to the direction of conduction. The thick blue lines represent the conducting layer, e.g., adsorbed water. The grain size is d_g, and the width (or diameter in the case of pores) is w_c. (For interpretation of the references to colour in this figure legend, the reader is referred to the web version of this article.)

$4w_c/d_g^2 = \psi_c$. The volume of pores in the unit volume – hence the relative porosity – is $p_r = w_c^2/d_g^2$. We then see that $\psi_c = 4w_c/d_g^2 = 4p_r/w_c = 4(1\text{-}\rho_r)/w_c$, where ρ_r is the relative density.

In a similar treatment for circular pore columns of width (diameter) w_c, the circumference is πw_c and the conductance of one column through one layer hence $\pi w_c G_s/d_g$. The conductance through a unit cube and hence macroscopic conductivity will be $\sigma_{M,c} = \pi w_c G_s/d_g^2 = \psi_c G_s$ and the volume specific surface area $A_v = \pi w_c/d_g^2$. The relative porosity is $p_r = \pi w_c^2/4d_g^2$ and we then see that $\psi_c = \pi w_c/d_g^2 = 4p_r/w_c = 4(1\text{-}\rho_r)/w_c$.

All in all, we may express the macroscopic materials conductivity in the direction of the columnar pores by the surface conductance and various parameters, including a unit-less geometry factor $\Psi_c = \psi_c w_c = 4p_r = 4(1\text{-}\rho_r)$ for columnar porosity:

$$\sigma_{M,c} = \frac{4p_r}{w_c}G_s = \frac{4(1-\rho_r)}{w_c}G_s = \frac{\Psi_c}{w_c}G_s = \psi_c G_s = A_v G_s \tag{6}$$

where $\psi_c = 4p_r/w_c = 4w_c/d_g^2$ for square columns and $\psi_c = 4p_r/w_c = \pi w_c/d_g^2$ for circular columns.

3.2.1.2. 3D structural porosity. Now, we add the volume of similarly penetrating pore columns in the two orthogonal directions. For small pores they will to a first approximation don't contribute to or obstruct conduction in the pores in the conducting direction. Similarly, the porosity is to a first approximation 3 times that of the 1D case, *i.e.*, $p_r = 3w_c^2/d_g^2$. Hence, the relationship between conductivity and porosity is affected with the same factor, and we get $\psi_c = 4w_c/d_g^2 = (4/3)p_r/w_c = (4/3)(1\text{-}\rho_r)/w_c$, and for this case $\Psi_c = (4/3)(1\text{-}\rho_r)$. In summary, the macroscopic materials conductivity for a case of open columnar porosity in the dimensions is

$$\sigma_{M,c} = \frac{4w_c}{d_g^2}G_s = \frac{4p_r}{3w_c}G_s = \frac{4(1-\rho_r)}{3w_c}G_s = \frac{\Psi_c}{w_c}G_s = \psi_c G_s \tag{7}$$

If the material is isotropic (cubic) and has open columnar porosity in all three directions, it does not matter in which direction the conductivity is measured due to the contributions from columns as they come into the driving electrical field.

This model may be appropriate for microporous materials such as zeolites and MOFs if the pores are large enough that a surface conductance can be defined in their structural pores. In reality, such materials are difficult to prepare as dense films or bulk samples, and may normally comprise inter-grain porosity like we will treat next in addition to the intra-grain structural porosity.

3.2.2. Materials with randomly connected pores

For more or less sintered powder compacts and porous ceramics, we may apply geometric models of varying sophistication to emulate and predict the macroscopic conductivity from the grain size, porosity, and surface conductivity. Here, we first present Gregori *et al.*'s brick layer model and show that it in essence is identical to the 1D columnar porosity model above, and then we present our own more generally applicable brick layer model and compare the different ones.

3.2.2.1. Gregori et al.'s brick layer model. Gregori *et al.* [18] studied protonic conductivity of a modestly porous binary oxide and proposed a brick layer model with proton transport in bulk, along grain boundaries, and in adsorbed layers and subsurface region of pores, see Fig. 2. They proposed that within certain realistic limits, a dominating pore surface conductivity gives rise to a macroscopic conductivity

$$\sigma_M = \beta\varphi_p\Omega a\sigma_{\infty,L} = \frac{4}{d}\varphi_p a\sigma_{\infty,L} = \frac{4}{d}\varphi_p G_s \tag{8}$$

where $\beta = 2/3$ in the brick layer model, φ_p is the open porosity volume fraction, $\Omega = 6/d$ is the surface-to-volume fraction of a pore of size d, and a and $\sigma_{\infty,L}$ are the thickness and volume conductivity of the water layer, respectively. The rightmost expression inserts our surface layer

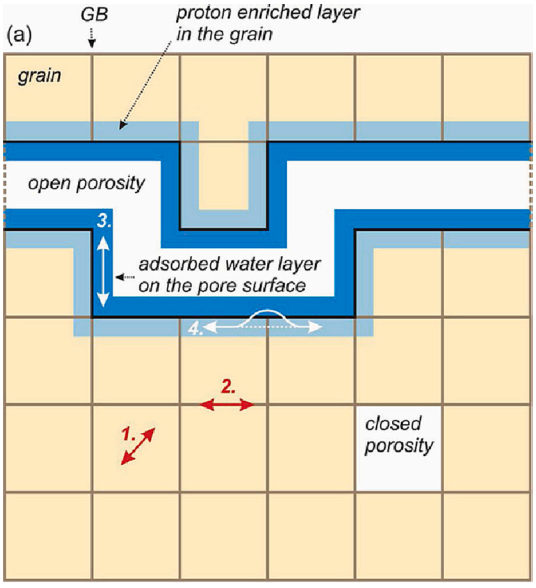

Fig. 2. Schematic 2D representation of the microstructure of four proton transport pathways in porous materials: 1 transport in the bulk, 2 along the GBs, 3 on the open pores surfaces in the adsorbed water layer, and 4 in a proton enriched subsurface layer. Copyright © 2013 WILEY-VCH Verlag GmbH & Co. KGaA, Weinheim. Reproduced from ref. [18] with permission.

conductance $G_s = a\sigma_{\infty,L}$, and inspection shows that it thereby has become equivalent to our 1D columnar model in Eq. 6. While it applies properly to truly 1D columnar porosity, the model comprises a simple proportionality to open porosity and is unsuited for larger porosities in materials with randomly organised porosity like compacted or sintered ceramics. This was also emphasised by Gregori *et al.* who applied it qualitatively to account for measured surface protonic conductivity in relatively dense sinters with low porosities, assuming that the protonic mobility in the adsorbed water was similar to that of the self-diffusion of H_3O^+ in water (~ $8\bullet10^{-3}$ cm^2/Vs at 200 °C).

3.2.2.2. A more general surface brick layer model (SBLM). Now, we derive a new surface brick layer model (SBLM) that is more generally applicable especially for highly porous compacted and sintered bodies. The geometry applied is the simplest possible, but for the benefit of the reader, we still provide and expand on the mathematics from the two articles where it first appeared. [19,20]

Let us divide the volume of a porous material with equal size d_g of grains and pores into cubic bricks of the same size d_g so that there are $1/d_g$ bricks in each unit length direction and $1/d_g^2$ per cross-sectional unit area, and $1/d_g^3$ bricks per unit volume. The bricks are statistically grains or pores, see Fig. 3 for schematic illustrations of cross-sectional planes with different porosities. The chance that a brick is a grain is proportional to the relative density ρ_r and hence related also to the relative porosity p_r of the material: $\rho_r = 1\text{-}p_r$.

In the direction of conduction, 4 of the 6 sides of a grain can contribute a conducting surface, and only if the neighbouring brick is a pore. The number of grain side surfaces in the **c**onducting direction through unit area of a **s**ingle **l**ayer of bricks is thus

$$n_{csl} = 4\rho_r p_r \frac{1}{d_g^2} = \frac{4\rho_r p_r}{d_g^2} = \frac{4\rho_r(1-\rho_r)}{d_g^2} \tag{9}$$

This is a simple function that goes through a maximum value at 50% relative density for which each brick contributes on average one conducting surface, *i.e.,* 2 per grain. We may insert $d_g = 1/6$ and calculate that microstructures with relative densities of 5/6, 1/2, and 1/3 like in Fig. 3, statistically should have, respectively, 20, 36, and 32 conducting sides.

The conductance through one layer is obtained by multiplying with the surface conductance of side sheets:

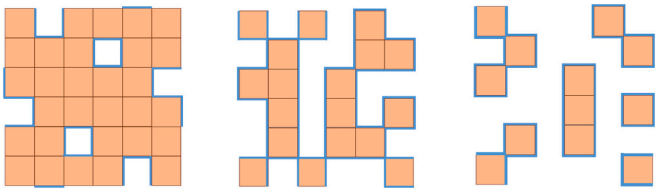

Fig. 3. Schematic single layers of 6 × 6 brick "random" porous microstructures viewed from above, into the direction of conduction through the plane of the image. Coloured bricks are grains and grain boundaries are the thin lines between them. Surfaces, e.g., with adsorbed water, are thick blue lines. Surfaces are drawn at the outer boundaries only where they would appear by expanding the same pattern in all four directions of the plane (in this way drawn differently than in the figure in the supplementary information of our paper on ZrO_2, [19] which it is adapted from). Densities are 5/6 (≈ 83%, left), 1/2 (50%, middle), and 1/3 (≈ 33%, right). Statistical numbers of conducting through-plane surfaces of the 6 × 6 brick layer according to the model we develop (Eq. 9, with $d_g = 1/6$) are 20, 36, and 32, while the actual numbers in a repeating matrix of the depicted "random" microstructures can be counted as, respectively, 24, 47, and 40. The difference to the model is assigned to the human rather than statistical selection of the example microstructures. (For interpretation of the references to colour in this figure legend, the reader is referred to the web version of this article.)

$$G_{sl} = G_s n_{csl} = G_s \frac{4\rho_r p_r}{d_g^2} = G_s \frac{4\rho_r(1-\rho_r)}{d_g^2} \tag{10}$$

Now, we apply the simplest possible consideration of percolation, *i.e.,* the probability that a surface through one layer coincides directly with another surface in the next layer, as illustrated schematically in Fig. 4. We take this probability to be the probability that an interface is a surface, namely, as before, $\rho_r p_r = \rho_r(1-\rho_r)$. Hence, the area specific number of connected conducting surfaces through one layer that percolates to the 1st next layer is reduced to

$$n_{csl\text{-}p1} = \frac{4\rho_r p_r}{d_g^2}\rho_r p_r = \frac{4\rho_r^2 p_r^2}{d_g^2} = \frac{4\rho_r^2(1-\rho_r)^2}{d_g^2} \tag{11}$$

and the conductance through this one layer is then correspondingly

$$G_{sL\text{-}p1} = G_s n_{csl\text{-}p1} = G_s \frac{4\rho_r^2 p_r^2}{d_g^2} = G_s \frac{4\rho_r^2(1-\rho_r)^2}{d_g^2} \tag{12}$$

This is still a simple function with maximum at a relative density of 50%, but now down at 0.25 conducting surfaces per brick, 0.5 per grain.

We might continue like this, making the straight percolating conduction path ever rarer, but orthogonal surfaces will immediately start to connect the ones we consider, and increase the conducting pathways. A numerical simulation of this could be useful, but the brick layer model is anyway crude. Generally, the power that the porosity and density are raised to, can be a variable ξ (xi) which we may call a percolation coefficient:

$$G_{sl\text{-}p\xi} = G_s n_{sl\text{-}p\xi} = G_s \frac{4(\rho_r p_r)^\xi}{d_g^2} = G_s \frac{4(\rho_r(1-\rho_r))^\xi}{d_g^2} \tag{13}$$

In reality, an isotropic microstructure of high porosity such as for powder compacts or poorly sintered ceramics will have well-connected pores and ξ probably close to 1 and certainly below 2, while low porosities and certain non-isotropic pore structures may have ξ above 2.

A unit volume will have a conductance divided by the number of layers of grains, *i.e.,* $1/d_g$, so that we get a macroscopic specific conductivity σ_M of the porous material of

$$\sigma_M = \frac{G_{sl\text{-}p\xi}}{\frac{1}{d_g}} = G_{sl\text{-}p\xi} d_g = G_s \frac{4\rho_r^\xi p_r^\xi}{d_g} = G_s \frac{4\rho_r^\xi(1-\rho_r)^\xi}{d_g} = \frac{\Psi}{d_g} G_s = \psi G_s \tag{14}$$

In this formula we recognise that the essential parameters for the conductivity of a randomly and highly porous material with surface conductance are the conductance G_s of the surface layer, the relative density ρ_r (or porosity p_r) and the grain (and pore) size d_g, while the percolation coefficient ξ expectedly in the range 1–2 plays an additional, but modest role. The unit-less factor Ψ is given as $\Psi = 4\rho_r^\xi p_r^\xi = 4\rho_r^\xi(1-\rho_r)^\xi$ in this simplified case of randomly porous materials.

The surface protonic conductivity of a simple porous material according to this model is inversely proportional to the grain size and has a maximum at 50% relative density of $\sigma_M = G_s/d_g$ for $\xi = 1$ and $0.25G_s/d_g$ for $\xi = 2$.

Fig. 5 shows a master plot of the unit-less factor Ψ as a function of relative density for the SBLM with $\xi = 1$, 1.5, and 2, compared with values for (1D) regular columnar and 3D columnar porosity. The SBLM handles in principle any relative density between 0 and 1, although too porous materials can hardly have mechanical integrity. The columnar models, however, are limited mathematically and realistically to high relative densities.

The SBLM handles to some extent closed porosity if $\xi > 1$, as can be realised from the concave shape of the conductivity curve near full density for $\xi = 1.5$ and 2. In considering square bricks, this however underestimates conductivity for less dense microstructures by not allowing conduction along facets connecting otherwise unconnected

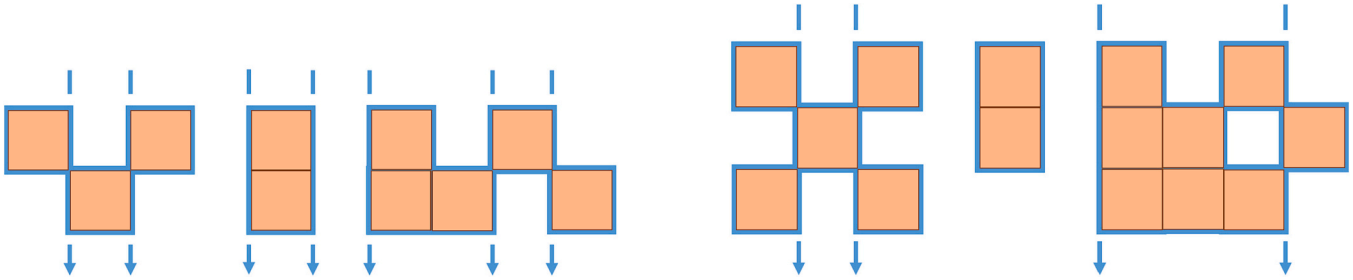

Fig. 4. Schematic side views of the vertical direction of conduction through 2-layer (left) and 3-layer (right) brick structures both with 10 vertical columns of bricks and 50% density by "random" population. The 2-layer example shows that out of the 10 surface sides in the top layer, only 7 surface sides percolate directly to another surface side in the next layer, marked with arrows. In the 3-layer example only 4 of these percolate in a straight manner further into the third layer. However, many paths circumvent this by use of orthogonal (horizontal) surfaces to another vertical path, which limits the exponential ξ of the probability in Eq. 13. Only one combination of grains (column 5, surfaces 5 and 6) leads to dead ends in our 3-layer example. The 3-layer example contains what appears in the 2D depiction to be a closed pore (column 9) that still contributes a percolating conducting surface, illustrating the mere statistical nature of the surface brick layer model.

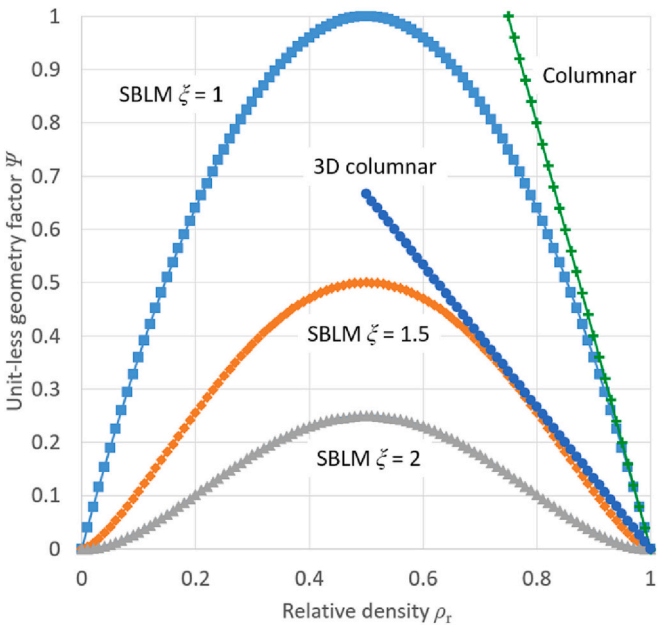

Fig. 5. Unit-less geometry factor Ψ for the SBLM for porous materials and Ψ_c for columnar porosity models as a function of relative density. The values of Ψ for the SBLM are calculated with percolation powers of $\xi = 1$, 1.5, and 2. The regular 1D columnar model coincides with that of Gregori *et al.* in ref. [18].

grain sides.

3.2.2.3. Estimating specific surface areas with the SBLM. In the regular (1D) columnar case we treated first, the proportionality ψ between materials conductivity and surface conductance was simply the volume-specific surface area A_v, as one can see from Eq. 6. For 3D randomly porous materials, the SBLM provides a simple efficient method of estimating the volume specific surface area from microstructural parameters, as derived in Ref. [19] (SI):

$$A_v = \frac{6\rho_r(1-\rho_r)}{d_g} \tag{15}$$

Inserting this, we obtain for the geometry factor ψ

$$\psi = \frac{4\rho_r^{\xi}(1-\rho_r)^{\xi}}{d_g} = \rho_r^{\xi-1}(1-\rho_r)^{\xi-1}\frac{4\rho_r(1-\rho_r)}{d_g} = \rho_r^{\xi-1}(1-\rho_r)^{\xi-1}\frac{2}{3}A_v \tag{16}$$

and in the assumption of $\xi = 1$, we obtain simply:

$$\psi = \frac{2}{3}A_v \tag{17}$$

We may at need convert between volume specific surface area A_v and gravimetric specific surface area A_g by

$$A_g = \frac{A_v}{\rho_p} = \frac{A_v}{\rho_r\rho_s} \tag{18}$$

where ρ_p and ρ_r are, respectively, the density and relative density of the porous material, and ρ_s is the theoretical density of the dense material.

All in all, the above expressions allow us to make first approximation estimates of volumetric and, in turn, gravimetric specific surface areas from the surface brick layer model. Conversely, we may use measurements of specific surface area by, e.g., BET analysis to estimate the geometry factor to convert between measured sample conductivity and surface conductance. Fig. 6 shows the order-of-magnitude correlation between gravimetric specific surface areas measured by BET and

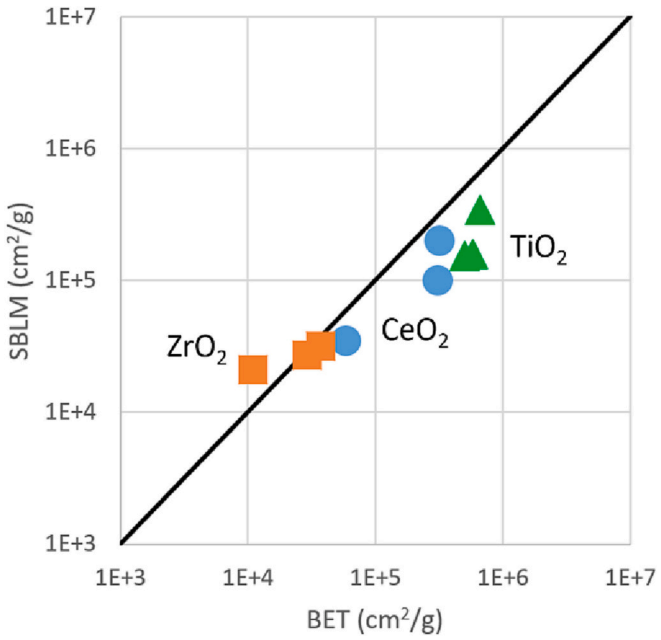

Fig. 6. Correlation between specific gravimetric surface areas from BET measurements and those calculated from the SBLM using Eq. 15 and Eq. 18 for powder and ceramic samples of ZrO_2, [19] CeO_2, [20] and TiO_2. [25] For the powder samples, a relative density of 50% was assumed, and for the plate-like and elongated crystallites in TiO_2 powders, the grain size was taken as the average between the long and short dimension.

calculated by the SBLM using Eq. 15 and Eq. 18 with data for oxide powders and ceramic samples from recent reports on surface protonic conduction.

3.2.2.4. Common features and general comments. Simple models like the ones presented here, including the SBLM, are crude, but serve to show a few general trends: The macroscopic conductivity is for all models directly proportional to the surface layer conductance, in turn given by the specific surface layer conductivity and its thickness. Moreover, it is inversely proportional to the grain and pore size. Finally, it is a function of the relative density. From the geometry of porous ceramics, we may expect macroscopic materials conductivities to have shallow peaks around 50% density at values corresponding to order of magnitude of $\sigma_M = G_s/d_g$, *i.e.,* the surface layer conductance in Siemens (S) divided by the grain and pore size.

There are to our knowledge no systematic experimental studies of surface conduction for a material over a large range of density and/or grain or pore size that would be able to test the validity of the proposed SBLM. Such studies would be much welcomed, and for now we must use the models with precaution. In the following, we will nevertheless review a few examples of their applicability for surface protonic conduction in porous ceramics, showing that they appear to apply within small variations of density and grain size for the same material, but more importantly, they allow order-of-magnitude distinction between types of adsorption and dissociation and proton migration.

3.2.3. Application to experimental surface protonic conductivities

3.2.3.1. Conduction in chemisorbed and physisorbed water. Water adsorbs on ionic solids in three distinguishable layers, chemisorbed (c), 1st solid-like physisorbed (p), and 2nd liquid-like physisorbed (p2). They come on with increasing coverage one by one, with increasing relative humidity (*RH*), *i.e.,* increasing partial pressure of water vapour p_{H_2O}, or decreasing temperature *T*, see Fig. 7. The adsorbed water dissociates to protonic charge carriers with different mobilities in the different layers, giving rise to surface protonic conduction. Each layer *L* has an in-plane surface conductance G_L given by its volume conductivity σ_L and the thickness t_L,

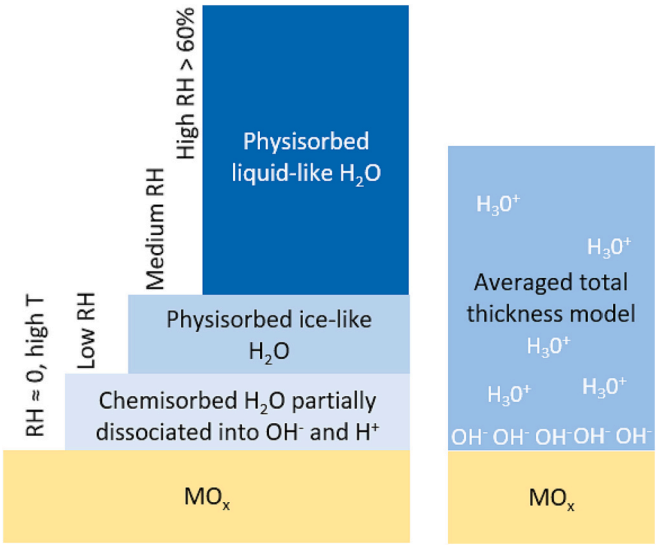

Fig. 7. Left: The three schematic layers of adsorbed water with typical classifications of *RH*. Right: Schematic example of an acidic oxide terminated preferentially by OH^- charge compensated by protons (H_3O^+) in the physisorbed layers and how the adsorbed layers in this case can be represented by a single total thickness layer with a conductivity given by the total concentration of protons and an averaged effective charge mobility. Adapted from ref. [25].

$$G_L = \sigma_L t_L \tag{19}$$

All three layers – to the extent that they are present – may be considered to contribute to the total surface conductance G_s:

$$G_s = G_c + G_p + G_{p2} \tag{20}$$

We consider next that the water layers make up a total thickness t_s and a total conductance G_s, for which we assign an effective (average) volume conductivity $\overline{\sigma_s}$ of protons:

$$\overline{\sigma_s} = \frac{G_s}{t_s} = \frac{G_c + G_p + G_{p2}}{t_c + t_p + t_{p2}} \tag{21}$$

Experimentally, we cannot delineate the three contributions directly, but variations in measured conductivity vs. for instance temperature can be fitted to Eq. 20 to obtain separate functions for the three, as applied by Kang *et al.* for TiO_2 nanomaterials. [25]

Alternatively, one may – in different regions of *T* and p_{H_2O} (different *RH*) – consider the outermost layer that is present completely dominating because it has proton mobility superior to the layer(s) underneath. Sun *et al.* [19,20] adopted this approach and were the first to develop it into quantitative models for proton migration mechanisms in the chemisorbed and 1st physisorbed layers. Within simplified assumptions of dominating adsorption and dissociation behaviours, low or full coverage, and predominant migration mechanisms, a surface conductance G_{s,H^+} could be expressed generally with a predictable standard preexponential G^0_{s,H^+0}, a given $p^n_{H_2O}$ dependency, and a single activation enthalpy of conductance $\Delta H_c = \Delta H^0 + \Delta H_{m,H^+}$ being a sum of standard enthalpies of adsorption and dissociation ΔH^0 and a migration activation enthalpy term $\Delta H_{m,H^+}$:

$$G_{s,H^+} = G^0_{s,H^+0}\left(\frac{p_{H_2O}}{p^0}\right)^n \frac{1}{T} exp\left(\frac{-\Delta H_c}{RT}\right) \tag{22}$$

Table 1 shows values of G^0_{s,H^+0} and *n* for the models evaluated. The thermodynamic cases for chemisorbed water are classified as molecular chemisorption with proton dissociation to surface oxide ions (cms-), dissociative chemisorption with proton dissociation to surface oxide ions (cds-), and molecular chemisorption with proton dissociation within the adsorbed layer (cma-). The transport mechanisms involve proton jumps between the surface oxide ions (−s), between surface oxide ions and adsorbed species (−sa), and between adsorbed species (−a). For the 1st physisorbed layer we consider protons from the chemisorbed layer underneath dissociated to and jumping in the physisorbed layer (cmp-p) and protons both dissociated and jumping within the 1st physisorbed layer (p-p). The papers by Sun *et al.* [19,20] provide more detailed descriptions and assumptions as well as schematics of the different mechanisms, while the abbreviations for the physisorbed layer here have been modified towards more consistency.

Sun *et al.* [19] parameterised conductivity data for porous ceramic samples of monoclinic ZrO_2 via the SBLM reviewed here. The grain sizes and relative densities yielded ψ values that were used to convert measured conductivities to surface conductances. Regression of Arrhenius plots in turn yielded preexponentials of protonic surface conductance that could be compared with predicted ones. For the surface protonic conductivity at relatively high temperatures, decreasing with temperature (positive activation enthalpies), there was good match with conduction in the chemisorbed layer (cms-s model). After use of the SBLM to remove the effect of different microstructures (grain size and porosity), the differences in surface conductance between samples sintered at different temperatures could be related to a tendency of stronger and more dissociative chemisorption (cds-s model) and with higher activation energy of proton migration for samples with more facetted surfaces (sintered at higher *T*). At lower measurement temperatures, the conductivity increased with decreasing temperature (apparent negative

Table 1
Derived p_{H_2O} dependences and predicted preexponentials (G^0_{s,H^+0} and G_{s,H^+0}) and activation enthalpies of surface protonic conductance (ΔH_c) within the chemisorbed water layer at p_{H_2O} = 1 bar (standard conditions) and 0.025 bar according to different models of dissociation and transport in cases of low coverage, for which molecular or dissociated chemisorption have the same parameters. Also included are predictions for full coverage, where there are no p_{H_2O} dependences, but differences between molecular or dissociated dominance. Note that models with transport between adsorbed species in the chemisorbed and physisorbed layers come out with the same preexponentials and have been tabulated together. Lines in Fig. 8 are based on the predicted preexponentials and empirical enthalpies in parenthesis. Adapted from ref. [20].

Model / Parameter	cms-s cds-s	cms-sa cds-sa	cms-a cds-a cmp-p	cma-a p-p	cms-s	cds-s	cms-sa	cds-sa	cms-a cmp-p	cds-a	cma-a p-p
n in $G_{s,H^+0} \propto p^n_{H_2O}$	1/2	1	3/2	2	0 (Full coverage)						
G^0_{s,H^+0} (SK), p_{H_2O}= 1 bar	$2\bullet10^{-6}$	$3\bullet10^{-9}$	$3\bullet10^{-12}$	$6\bullet10^{-15}$	$1\bullet10^{-3}$	$4\bullet10^{-4}$	$1.5\bullet10^{-3}$	$8\bullet10^{-4}$	$1\bullet10^{-3}$	$8\bullet10^{-4}$	$1.5\bullet10^{-3}$
G_{s,H^+0} (SK), p_{H_2O}= 0.025 bar	$2\bullet10^{-7}$	$8\bullet10^{-11}$	$1\bullet10^{-14}$	$4\bullet10^{-18}$	$1\bullet10^{-3}$	$4\bullet10^{-4}$	$1.5\bullet10^{-3}$	$8\bullet10^{-4}$	$1\bullet10^{-3}$	$8\bullet10^{-4}$	$1.5\bullet10^{-3}$
ΔH_c (kJ/mol) (plotted in Fig. 8)	+30 (+29)	0 (−10)	−60 (−45)	−70	+60	+50	+60	+40	+30 (+25)	0	+40

activation enthalpy). The thermodynamic model of adsorption and dissociation and the corresponding mechanisms of migration within the adsorbed layer could for the first time rationalise such enthalpies, and predicted preexponentials many orders of magnitude lower for conduction in the physisorbed than in the chemisorbed layer. This was shown again to fit well to the experimental ones via the SBLM and was attributed to physisorbed water and what we here abbreviate the cmp-p and p-p protonic transport mechanisms.

In a subsequent study of nanoscopic porous CeO_2, Sun *et al.* [20] built on the model from the ZrO_2 paper, but the hydrophobic nature of CeO_2 (attributed to a hydrogenated CeOOH-like surface region) showed – via a range of sorption and thermogravimetry measurements – that an extended set of migration models for the chemisorbed layer was needed, abbreviated cds-sa and cms-a models. The surface conductances in wet atmosphere for two samples sintered at 550 and 750 °C are shown in Fig. 8. As seen, the sample surface conductivity that was considerably higher for the finer more porous sample sintered at 550 °C (ρ_r = 50%) becomes roughly equal to the coarser 750 °C sample (ρ_r = 62%) in terms of the surface conductance via the SBLM.

It should be noted that in the work on ZrO_2 the extraction of preexponentials and enthalpies was done by normal regression of Arrhenius plots and then compared with model values. [19] As a different approach, Fig. 8 for CeO_2 has trend lines drawn by fixing the preexponentials to the predicted model values and then the slope and hence empirical enthalpies are obtained by rotating the line to fit the relevant range of surface conductances. [20].

4. Summarising conclusions

We have for compacts and sinters with high open porosity derived a surface brick layer model (SBLM) to mathematically connect the surface conductance G_s in Siemens (S) and the macroscopic surface conductivity $\sigma_{M,s}$ of the porous material by use of a choice of parameters expressing the material's microstructure:

$$\sigma_{M,s} = \frac{4\rho_r^{\xi} p_r^{\xi}}{d_g} G_s = \frac{4\rho_r^{\xi}(1-\rho_r)^{\xi}}{d_g} G_s = \frac{\Psi}{d_g} G_s = \psi G_s = \rho_r^{\xi-1}(1-\rho_r)^{\xi-1}\frac{2}{3} A_v G_s \quad (23)$$

Here, ρ_r and p_r are relative density and porosity, respectively, d_g is the size of the grains and pores, and Ψ is a unit-less geometry factor and ψ is the same factor divided by the grain size. The volume-specific surface area A_v can replace porosity and density and grain size. The exponent ξ expresses the obstacle of percolation and can in our opinion be left at 1 for simplicity, or increased to e.g., 1.5 or maximum 2 for less porous and more anisotropic microstructures, without affecting the order-of-magnitude limitation the crude model anyway represents.

For 1D columnar porosity, a more accurate version applies,

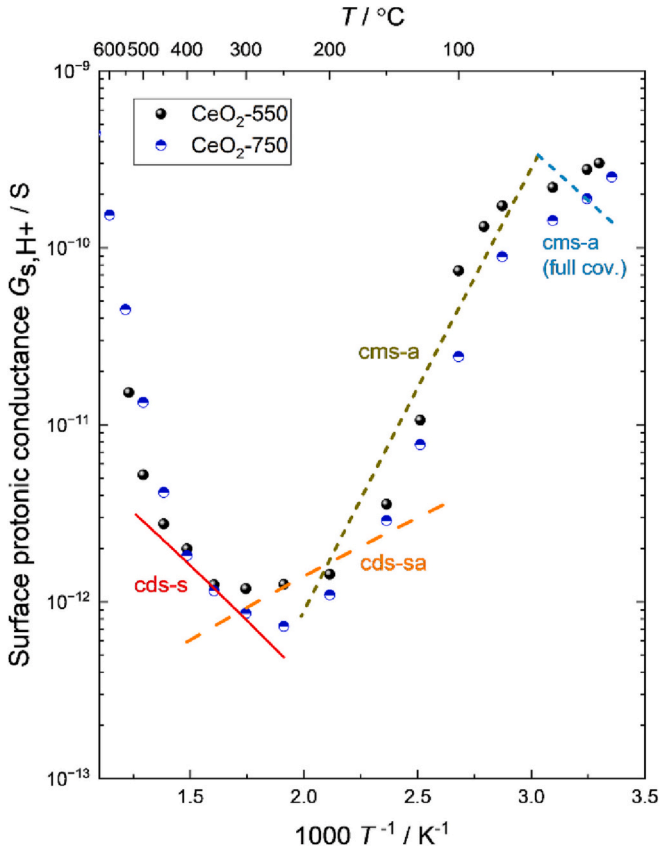

Fig. 8. Surface protonic conductance of two CeO_2 samples sintered at 550 (ρ_r = 50%) and 750 °C (ρ_r = 62%) vs $1/T$ in wet (p_{H_2O} = 0.025 bar) N_2, obtained from the sample conductivities via the SBLM. The lines are drawn using preexponentials derived for models cds-s, cds-ca, and cms-a in the cases of low coverage, the latter with an extension also to full coverage, see Table 1. Reproduced from ref. [20] under Creative Commons CC-BY. © 2022 The Author (s). Published by Elsevier B.V.

$$\sigma_{M,c} = \frac{4p_r}{w_c} G_s = \frac{4(1-\rho_r)}{w_c} G_s = \frac{\Psi_c}{w_c} G_s = \psi_c G_s = A_v G_s \quad (24)$$

where w_c is the width of a square pore, and similar expressions for other 1D pore cross-sections can be derived in a straightforwardly manner. An approximate model for materials with 3D orthogonal columnar pores is suggested for surface conduction in the structural porosity of so-called microporous materials like zeolites and MOFs.

We have exemplified how different models for chemisorption and physisorption of water, dissociation, and migration of protons lead to expressions for surface proton conduction $G_{s,H+}$ with quantifiable pre-exponentials, and we have reviewed results from recent literature on nanoporous ZrO_2 and CeO_2 showing that credible models fit experimental preexponentials within order-of-magnitude via the SBLM.

CRediT authorship contribution statement

Truls Norby: Conceptualization, Writing – original draft, Writing – review & editing, Visualization, Supervision, Project administration, Funding acquisition. **Xinwei Sun:** Investigation, Writing – review & editing, Visualization. **Einar Vøllestad:** Writing – review & editing, Supervision.

Declaration of Competing Interest

The authors declare no competing interests.

Data availability

Data will be made available on request.

Acknowledgements

This work has been supported by the Research Council of Norway (RCN) through projects MoZEES (257653) and SUPROX (280868).

References

[1] Y. Hisai, et al., Enhanced activity of catalysts on substrates with surface protonic current in an electrical field - a review, Chem. Commun. 57 (47) (2021) 5737–5749.
[2] R. Manabe, et al., Surface protonics promotes catalysis, Sci. Rep. 6 (1) (2016) 1–7.
[3] M. Torimoto, K. Murakami, Y. Sekine, Low-temperature heterogeneous catalytic reaction by surface protonics, Bull. Chem. Soc. Jpn. 92 (10) (2019) 1785–1792.
[4] X.L. Kang, et al., Water vapor photoelectrolysis in a solid-state photoelectrochemical cell with TiO_2 nanotubes loaded with CdS and CdSe nanoparticles, ACS Appl. Mater. Interfaces 13 (39) (2021) 46875–46885.
[5] K. Xu, et al., Hydrogen from wet air and sunlight in a tandem photoelectrochemical cell, Int. J. Hydrog. Energy 44 (2) (2019) 587–593.
[6] D. Poetzsch, R. Merkle, J. Maier, Oxygen reduction at dense thin-film microelectrodes on a proton-conducting electrolyte: I. considerations on reaction mechanism and electronic leakage effects, J. Electrochem. Soc. 162 (9) (2015) F939.
[7] E. Vøllestad, et al., Mixed proton and electron conducting double perovskite anodes for stable and efficient tubular proton ceramic electrolysers, Nat. Mater. 18 (7) (2019) 752–759.
[8] S.Ø. Stub, Protonic Conduction in Porous Oxides, in: Department of Chemistry, Faculty of Mathematics and Natural Sciences, University of Oslo, Oslo, 2017, p. 85.
[9] P. Simons, et al., A ceramic-electrolyte glucose fuel cell for implantable electronics, Adv. Mater. 34 (24) (2022) 2109075.
[10] S. Kim, et al., Unprecedented room-temperature electrical power generation using nanoscale fluorite-structured oxide electrolytes, Adv. Mater. 20 (3) (2008) 556–559.
[11] M.T. Colomer, Nanoporous anatase ceramic membranes as fast-proton-conducting materials, J. Eur. Ceram. Soc. 26 (7) (2006) 1231–1236.
[12] L. Almar, et al., Mesoporous ceramic oxides as humidity sensors: A case study for gadolinium-doped ceria, Sens. Actuat. B-Chem. 216 (2015) 41–48.
[13] J. Wang, et al., Sensitivity and complex impedance of nanometer zirconia thick film humidity sensors, Sens. Actuat. B-Chem. 139 (2) (2009) 418–424.
[14] M. Onen, et al., Nanosecond protonic programmable resistors for analog deep learning, Science 377 (6605) (2022) 539–543.
[15] S.Ø. Stub, E. Vøllestad, T. Norby, Mechanisms of protonic surface transport in porous oxides: example of YSZ, J. Phys. Chem. C 121 (23) (2017) 12817–12825.
[16] S.Ø. Stub, E. Vøllestad, T. Norby, Protonic surface conduction controlled by space charge of intersecting grain boundaries in porous ceramics, J. Mater. Chem. A 6 (18) (2018) 8265–8270.
[17] S. Raz, et al., Characterization of adsorbed water layers on Y_2O_3-doped ZrO_2, Solid State Ionics 143 (2) (2001) 181–204.
[18] G. Gregori, M. Shirpour, J. Maier, Proton conduction in dense and porous nanocrystalline ceria thin films, Adv. Funct. Mater. 23 (47) (2013) 5861–5867.
[19] X.W. Sun, et al., Quantifiable models for surface protonic conductivity in porous oxides - case of monoclinic ZrO_2, Phys. Chem. Chem. Phys. 24 (2022) 11856–11871.
[20] X. Sun, et al., Surface protonic conductivity in chemisorbed water in porous nanoscopic CeO_2, Appl. Surf. Sci. 611 (2023), 155590.
[21] J. Maier, Space charge regions in solid two phase systems and their conduction contribution — II Contact equilibrium at the interface of two ionic conductors and the related conductivity effect, Ber. Bunsenges. Phys. Chem. 89 (4) (1985) 355–362.
[22] J. Maier, Ionic conduction in space charge regions, Prog. Solid State Chem. 23 (3) (1995) 171–263.
[23] N.J. Kidner, et al., Impedance/dielectric spectroscopy of electroceramics–Part 1: evaluation of composite models for polycrystalline ceramics, J. Electroceram. 14 (3) (2005) 283–291.
[24] S.M. Haile, D.L. West, J. Campbell, The role of microstructure and processing on the proton conducting properties of gadolinium-doped barium cerate, J. Mater. Res. 13 (6) (1998) 1576–1595.
[25] X.L. Kang, et al., Facet-engineered TiO_2 nanomaterials reveal the role of water-oxide interactions in surface protonic conduction, J. Mater. Chem. A 10 (1) (2022) 218–227.